Catena 157 (2017) 344–356

Contents lists available at ScienceDirect

Catena

journal homepage: www.elsevier.com/locate/catena

Effects of time step length and positioning location on ring-measured infiltration rate

Jing Zhang[a], Tingwu Lei[a,b,*], Zhe Yin[a], Yaqi Hu[a], Xiusheng Yang[c]

[a] College of Water Resources & Civil Engineering, China Agricultural University, Beijing 100083,PR China
[b] State Key Laboratory of Soil Erosion and Dryland Farming on the Loess Plateau, Institute of Soil and Water Conservation, CAS and MWR, Yangling, Shaanxi 712100, PR China
[c] Department of Natural Resources and the Environment, University of Connecticut, Storrs, CT 06269, USA

ARTICLE INFO

Keywords:
Time step length
Positioning location
Ring infiltrometer
Soil infiltration rate

ABSTRACT

Soil infiltration, an important component of hillslope hydrology, is widely measured with ring infiltrometers. In the numerical algorithms used for soil infiltration measurement, the time step length (STL) for reading water level and positioning location (PL) of average infiltration rates within a time step considerably affect the measured infiltration rate curves. In this study, four TSLs (1, 2, 5 and 10 min) were used to record falling water depth and three PLs (initial, mid, and end points of the time step) were applied to position the measured average infiltration rate, to evaluate the effects of TSL and PL on the measurement accuracy of infiltration rate. For a specific TSL, three infiltration rate curves were obtained by positioning the average infiltration rate at initial point (f_i), midpoint (f_m), and end point (f_e), respectively. Results show that the infiltration rates of f_e increases with TSL increasing. A short TSL reduces measurement errors caused by the TSL. However, a short TSL produces high measurement errors caused by reading the Mariotte bottle scale and increases practical difficulties. The f_m of different TSL were the closest to the true soil infiltration process, regardless of the TSL (i.e. 2, 5 or 10 min), with a maximum error in cumulative infiltration of approximately 11.14%. The TSL could be reasonably long, such as 5 or 10 min, as long as the measured average infiltration rates are positioned at the midpoint of a TSL. This strategy can avoid short-time measurement errors and reduce operational difficulties.

1. Introduction

Infiltration is the process of water entering soil and generally referred to as the downward movement of water from the soil surface (Bouwer, 1986; Hillel, 1998). This process affects the transport route of chemicals, the water quality of agricultural drainage, and the uniformity and efficiency of surface irrigation (Berehe et al., 2013; Rashidi et al., 2014). Infiltration rates influence the timing of overland flow (Jury and Horton, 2004; Viessman and Lewis, 1995). In addition the actual soil infiltration and rainfall intensity determine the runoff volume (Philip and Wayne, 2002). Infiltration rate is an important component of any hydrologic model (Viessman and Lewis, 1995).

Among the numerous tools for soil infiltration measurement (Bouwer, 1986; Lei et al., 2006a,b; Ogden et al., 1997; Peterson and Bubenzer, 1986; Perroux and White, 1988), the double-ring infiltrometer described by Bouwer (1986) is the most commonly used method to determine soil infiltration and soil hydraulic properties (Bagarello and Sgroi, 2004; Iwanek, 2008; Neris et al., 2012; Verbist et al., 2013).

A complete infiltration curve measured with a ring infiltrometer is calculated using the average infiltration rate during a certain period before being positioned at the end point of the TSL. Therefore, determining the optimum TSL before measuring an infiltration curve is important to obtain accurate measurement results. ASTM (2003) suggests the use of a 15-min TSL for the first hour and 30 min for the second hour. Eijkelkamp Company (2012) also proposed that the decrease in water level in the inner ring must be determined using 1–2 min intervals in the initial infiltration stage and using with a 20–30 min intervals in the subsequent stages. Standards have not been unified regarding the optimum TSL required for ring infiltrometers used in different soils. Therefore, scientists use different TSL to measure soil infiltration rates. For example, Bagarello and Sgroi (2004) and Mao et al. (2008) used 2 min intervals by monitoring the decrease in water level in an infiltrometer reservoir. Peng et al. (2015) calculated the infiltration rate by using 2 min intervals for the first 10 min and 5 min intervals for 10–90 min to study the effect of urbanization on water retention. Woltemade (2010) also calculated the infiltration rate by using 15 min intervals to study the effect of residential soil disturbance

* Corresponding author at: China Agricultural University, No. 17, Qinghua Donglu Rd, Haidian District, Beijing 100083, PR China.
E-mail address: leitingwu@cau.edu.cn (T. Lei).

http://dx.doi.org/10.1016/j.catena.2017.05.013
Received 7 November 2015; Received in revised form 13 May 2017; Accepted 15 May 2017
Available online 05 June 2017
0341-8162/ © 2017 Published by Elsevier B.V.

on infiltration rate and storm water runoff. Carlier (2007) used a 3 min TSL to measure the soil infiltration. Anari et al. (2011), Adindu Ruth. et al. (2014), Champatiray (2014), Oshunsanya (2013), Rasaily et al. (2014) and Uloma et al. (2014), calculated infiltration rates by using 5 min intervals. In their studies, the average infiltration rates were all positioned at the end point of the TSL of measurement.

The infiltration rate curves of different soils follow the same trend, which is that soil infiltration is relatively high in the initial stage, rapidly decreases with time, and gradually settles to a steady infiltration rate. Soil infiltration rate curves continuously change over time (Jury and Horton, 2004) and can be described by Green and Ampt (1911), Kostiakov (1932), Horton (1941) and Philip (1954) models. Obtaining the average infiltration rate (the measured infiltration rate during a fixed interval), instead of the transient infiltration rate (the soil infiltration rate at a given moment within the interval), during a time period before positioning at the end of the TSL causes the measured infiltration curve to deviate from the actual curve and thus produces a system error in the infiltration rate measurement.

Scientists have adopted different strategies, such as a water level sensor or a water depth sensor, to improve the measurement accuracy of the supplied water flow (Constantz and Murphy, 1987; Prieksat et al., 1992; Maheshwari, 1996). These methods have not been widely adopted by the scientific community possibly because of their relative high cost and complexity. Therefore, the traditional method of reading a tape measure for the supplied water flow is still commonly used to determine soil infiltration by a ring infiltrometer (Bodhinayake et al., 2004; Bagarello et al., 2009; Bamutaze et al., 2010; Chowdary et al., 2006; Lai and Ren, 2007; Ries and Hirt, 2008; Ruggenthaler et al., 2015). In an attempt to reduce the measurement errors caused by the measurement TSL, scientists tried to use shorter intervals at the initial stage of infiltration. León et al. (2015) suggested that readings should be performed at a TSL of 0.5 min. The use of a short TSL may reduce the measurement errors and improve the calculation accuracy. However, this method causes observation difficulties to a certain extent, and introduces measurement errors resulting from the difficulties in accurately reading the scale of the water supply tank. The water level in the ring or Mariotte bottle minimally changes within a short time step. Thus, a short time step may not be ideal.

To measure the infiltration accurately, the influence of different TSL and PL on measurement accuracy should be quantitatively evaluated. Accordingly, this study aimed to: 1) quantitatively estimate the effects of TSL and PL on measured soil infiltration curves, 2) estimate the measurement error under different TSLs and PLs on the basis of water balance, and 3) propose the optimal PL for measurements using ring infiltrometers.

2. Theory

A ring infiltrometer works based on the following assumption: the infiltration rate curves at different spatial locations follow the same decreasing function over time. The Mariotte bottle supplies water for ring infiltrometers at varied rates to maintain a constant water level in the ring. The infiltration water flow is calculated based on the changing water level in the Mariotte bottle. The infiltration rate is then calculated based on the changing water flow rates given by:

$$i(t) = q(t)/A \tag{1}$$

where $q(t)$ is the transient water flow rate of a Mariotte bottle, $L^3\,T^{-1}$; $i(t)$ is the infiltration rate, $L\,T^{-1}$; and A is the area of the ring, L^2.

2.1. Effect of TSL on infiltration curve

The instantaneous $q(t)$ in Eq. (1) is theoretical which is unachievable in actual water supply processes. Instead of the transient water flow rate, the average flow rate is used during practical measurement in a given time period:

$$\bar{q}_j = \frac{Q_j - Q_{j-1}}{\Delta t_j} = \frac{1}{t_j - t_{j-1}} \int_{t_{j-1}}^{t_j} q(t)dt \tag{2}$$

where $\bar{q}_j$ is the average flow rate during the period of $t_j - t_{j-1}$, $L^3\,T^{-1}$; Q_{j-1} and Q_j are the amounts of water in the Mariotte bottle at time moments t_{j-1} and t_j respectively, L^3; Δt_j is the TSL, T.

In consideration of the average flow rate at a specific TSL, the average infiltration rate is given as:

$$\bar{i}_j = \frac{\bar{q}_j}{A} = \frac{1}{A(t_j - t_{j-1})} \int_{t_{j-1}}^{t_j} q(t)dt \tag{3}$$

where $\bar{i}_j$ is the average infiltration rate in the period $t_j - t_{j-1}$, $L\,T^{-1}$; and A is the area of the infiltration ring, L^2.

According to the integral mean value theorem, Eq. (3) can be transformed into:

$$\bar{i}_j = i(t_\zeta) = \frac{\bar{q}_j}{A} = \frac{1}{A(t_j - t_{j-1})} \int_{t_{j-1}}^{t_j} q(t)dt = \frac{q(t_\zeta)}{A} \quad (t_{j-1} < t_\zeta < t_j) \tag{4}$$

where t_ζ is the time at which the accurate infiltration rate is positioned (the true soil infiltration rate under ideal conditions compared with the measured values), T; and $\bar{i}_j$ located at a moment between t_{j-1} and t_j is reached.

In the literature (Kumar, 2014; Mao et al., 2008; Peng et al., 2015; Rasaily et al., 2014), the average infiltration rate ($\bar{i}_j$) is positioned at the end of the TSL (Conventional PL in Fig. 2). Hence, the coordinate of the infiltration curve at time t_j is (t_j, $\bar{i}_j$). The infiltration process $i(t)$ is the monotone function of time t; thus $i(t_j) < \bar{i}_j < i(t_{j-1})$. The measured infiltration curve is higher than the natural value when $\bar{i}_j$, instead of $i(t_j)$, is placed at the end moment of the TSL; hence, system measurement errors are produced.

Fig. 1 presents three infiltration curves: the first curve is the probable true infiltration curve (the probable correct value positioned at the right moment) and the two other curves are the infiltration curves measured at dt_1 and dt_2 TSL ($dt_2 > dt_1$). As shown in Fig. 1, the measured infiltration rate is higher than the actual value when positioned at the end point of time step. The infiltration curve measured at dt_2 TSL is higher than that measured at dt_1 ($dt_1 < dt_2$) TSL. In this case, $\bar{i}_1$ and $\bar{i}_2$ are the average infiltration rates measured at dt_1 and dt_2 TSL, respectively. Moreover, $\bar{i}_1$ is larger than $\bar{i}_2$, indicating that the measured average infiltration rate increases with decreasing TSL. The infiltration curve determined at dt_1 approximates the probably actual curve better than that determined at dt_2. The system measurement error decreases

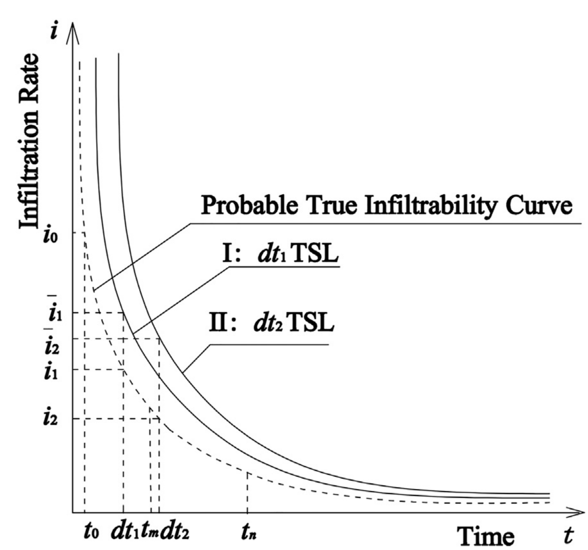

Fig. 1. Effect of different TSLs on the measured infiltration rates (note: I is the infiltration rate curve measured at dt_1; II is the infiltration rate curve measured at dt_2).

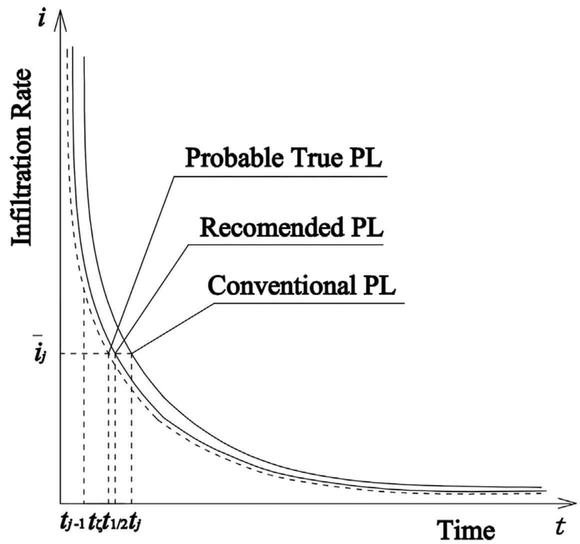

Fig. 2. Comparison of infiltration curves at different PL (note: $t_j - t_{j-1}$ is the TSL; $\bar{i}_j$ is the average infiltration rate in the TSL; probable true PL is the point (t_ζ) which is the probable accurate time coordinate for the average infiltration rate $\bar{i}_j$ during the TSL. Recommended PL is the midpoint ($t_{1/2}$) of the TSL. Conventional PL is the end point (t_j) of the TSL).

with decreasing TSL. When the TSL infinitely decreases, the measured infiltration curve infinitely approaches to the actual curve and the system measurement error infinitely approaches zero. However, decreasing the TSL may increase operational difficulty and is sometimes unachievable.

2.2. Effect of PL on infiltration curve

In Section 2.1, PL at the end of time step produces a higher infiltration curve than the actual soil infiltration. In Eq. (4), the average infiltration rate of a period from t_{j-1} to t_j represents the transient infiltration rate at time $t_\zeta (t_{j-1} < t_\zeta < t_j)$, as shown in Fig. 2. In actual operations, obtaining the accurate/exact PL, t_ζ on the time coordinate, is theoretically difficult. The midpoint of the TSL is a good approximation of the moment t_ζ, especially when the infiltration curve changes nearly linearly at its initial stage. Thus using the midpoint of the TSL instead of time t_ζ can result in the measured infiltration curve to approximate the probable true curve (Fig. 2). As the midpoint of the TSL replaces the end point, the infiltration curve moves to the left for half a unit of the TSL on the time coordinate. As a result, the measured infiltration curve is close to the actual curve and the system measurement error is reduced to a minimum degree. Thus, adopting the appropriate TSL and using the midpoint of the TSL as the PL can simplify the measurement procedure and provide high accuracy.

2.3. Measurement and model presentation of infiltration curve

Several models have been proposed based on the infiltration experimental data to represent the soil infiltration–time function. Two of the most popular infiltration models include the Kostiakov and the Philip infiltration models.

The Kostiakov infiltration model is derived from a large number of experimental infiltration rates. The parameters in this model bear no physical meaning but empirical constants. The Kostiakov infiltration model is given as:

$$i = at^{-b} \tag{5}$$

where i is the infiltration rate, L T^{-1}, and a and b are the fitted parameters.

Philip (1958, 1957a,b) solved the Richard partial differential equation for unsaturated water flows by using the first two terms of the power series to obtain the Philip model:

$$i = i_\infty + 0.5St^{-0.5} \tag{6}$$

where S and i_∞ are fitted parameters. i_∞ is conceptually the final state infiltration rate, L T^{-1}; and S is the sorptivity, L $T^{-1/2}$.

The Kostiakov and Philip models can be unified to represent the infiltration process, given by:

$$(i - i_\infty)^A \times (t - t_0)^B = c \tag{7}$$

where i_∞ is the final infiltration rate, L T^{-1}; t_0 is the start time of infiltration, T; A, B and c are constants.

Eq. (7) can also be transformed into:

$$\begin{aligned} &(i - i_\infty)^A \times (t - t_0)^B = c \\ &i - i_\infty = c^{1/A} \times (t - t_0)^{-B/A} \\ &i = i_\infty + c^{1/A} \times (t - t_0)^{-B/A} \end{aligned} \tag{8}$$

When i_∞ and t_0 are zero, B/A is $-b$, and c equals a, Eq. (8) is equivalent to Eq. (5), as Kostiakov model. When $c^{1/A}$ equals 0.5 S, t_0 is zero and B/A is 0.5, Eq. (8) is equivalent to Eq. (6), as Philip model. Thus, the Kostiakov and Philip models can be unified using Eq. (8). Therefore, the Kostiakov and Philip models are indeed the same hyperbolic function (Fig. 1).

Eq. (8) indicates that the soil infiltration rate is initially high and then rapidly decreases with time. The infiltration curve is approximately linear in the early infiltration stage. Toward the end, the infiltration rate decreases slowly with time and becomes nearly linearly correlated with time. Thus, the infiltration curve could be simplified into three parts: the first section can be approximated with a linear line (from 0 to t_m, Fig. 1), the intermediate part is a concave curve (from t_m to t_n, Fig. 1), and the last section can also be approximated with linear line (from t_n to t_∞, Fig. 1). When the infiltration process is located in the section where it is nearly linearly correlated with time, the average infiltration rate at a specific TSL closely approximates the actual infiltration rate at the TSL midpoint. Thus, the midpoint of the TSL closely approaches t_ζ, and locating the measured infiltration curve to this location well approximates the true infiltration curve. In the concave part of the infiltration curve, the average infiltration rate positioned at the midpoint of the TSL may deviate from that at t_ζ and may have a measurement error.

3. Materials and methods

3.1. Experimental materials

Experiments were conducted with a ring infiltrometer imitation, made of a plexiglass tube (30 cm diameter, 65 cm height). Holes of 1 cm diameter were drilled at the bottom of the ring to act as an air leak and water drainage boundary passages. Three soil types were collected from different regions in China. Soil S1, containing 15.0% clay, 50.2% silt, and 34.8% sand particles, was collected from Beijing. Soil S2, containing 21.2% clay, 65.7% silt, 13.1% sand particles was collected from Ansai, Shanxi province in northwestern China. And Soil S3, containing 34.3% clay, 63.2% silt, 2.5% sand particles, was collected from Jiangxi province in southeastern China. The soil materials were air-dried (2.5% g/g soil moisture content) and visible organic residues were removed. Then the soil materials were gently crushed by hand to pass through a 4 mm mesh and were mixed with sprayed water to attain a moisture content of approximately 10%, which was approximately 30–40% of the field capacity of the soil. The calculated soil materials of a 5 cm thickness based on the soil bulk densities were weighted with an electronic balance. The weighted soil materials were then packed uniformly into the ring infiltrometer and gently compacted to a thickness of 5 cm thickness by rakes. Before adding the next layer, the previously packed soil layer surface was scrubbed rough to prevent discontinuity between the two adjacent layers. Soil materials were packed into bulk densities of 1.2, 1.3 and 1.4 g cm^{-3}. The overall depth of soil in the ring infiltrometer was 60 cm, which is sufficient for the infiltration experiment to run for at least 2 h. This soil depth can be found typically in the Loess regions of the Northwestern China and the North China Plain (Lai and Ren, 2007; Hou et al., 2012).

The Mariotte bottles were made of plexiglass cylinders, 21 cm in diameter and 130 cm in height to supply a changing flow rate for the ring infiltrometer to maintain a constant water level.

3.2. Experimental method

The initial soil infiltration of soil S1 is typically high and needs a high rate of water flow to make measurements. The water supply capacity of the Mariotte bottle was limited by the flow capability; thus, sufficient water flow could not be supplied to meet the requirement of soil infiltration. Therefore, the initial infiltration rate of soil S1 was measured using the "falling head" method. A nylon cloth was placed on the soil surface within the ring to prevent scouring when water was poured into the ring at the beginning of the experiment. The computed amount of water equivalent to 4 cm depth in the ring was weighed using an electronic balance with a precision of 0.01 g before pouring into the ring as quickly as possible and starting the stopwatch to record time.

When the depth of the water level in the ring was 1 cm, water was added to a depth of 3 cm in the ring and the water outlet of the Mariotte bottle was immediately placed inside the ring under water. The Mariotte bottle started to supply water immediately until the end of the experiment. For soil S2 and soil S3, the water that infiltrated throughout the infiltration process was supplied by a Mariotte bottle. Before the experiment, the correct height of the air inlet of the Mariotte bottle was adjusted to supply the water flow into the ring to maintain a water depth of 3 cm on the soil surface. The water level change for each treatment was recorded at TSL of 1, 2, 5 and 10 min, respectively. After 30 min from the start of the experiment, the water level in the Mariotte bottle changed slowly at a 1 min TSL. The accurate reading of the water level in 1 min intervals was difficult; thus the TSL was adjusted to 2 min. Each treatment was repeated three times.

The average infiltration rate was calculated by TSL of 1, 2, 5, 10 min, as follows:

$$\bar{i} = \frac{\Delta H A_m}{A \Delta t} \times 600 \tag{9}$$

where $\bar{i}$ is the measured average infiltration rate, mm h^{-1}; ΔH is the supplied water at a TSL of 1, 2, 5, or 10 min, cm; A_m is the area of the Mariotte bottle, cm^2; A is the area of the infiltration ring, cm^2; Δt is the TSL (1, 2, 5, or 10 min); and 600 is the conversion coefficient, to convert cm min^{-1} into mm h^{-1}.

For a specific TSL, the average infiltration rate could be positioned at three time moments of TSL. Then, three infiltration curves can be obtained, as shown in Eq. (10):

$$i_m(t) = \begin{cases} f_i = \bar{i}(\Delta t_i) \\ f_m = \bar{i}(\Delta t_m) \\ f_e = \bar{i}(\Delta t_e) \end{cases} \tag{10}$$

where Δt is the TSL; $i_m(t)$ is the measured infiltration rate by Δt; f_i is the infiltration rate curve determined by positioning the average infiltration rate to the initial point of Δt; Δt_i is the initial point of Δt; f_m is the infiltration rate curve by positioning the average infiltration rate to the mid-point of Δt; Δt_m is the mid-point of Δt; f_e is the infiltration rate curve by positioning the average infiltration rate to the end point of Δt; Δt_e is the end point of Δt.

Then the infiltration rate curves, except for 1 min TSL during the first 30 min, were fitted to the Kostiakov and Philip models to further assess the effects of TSL and PL on the accuracy of infiltration rate measurements (Fig. 3).

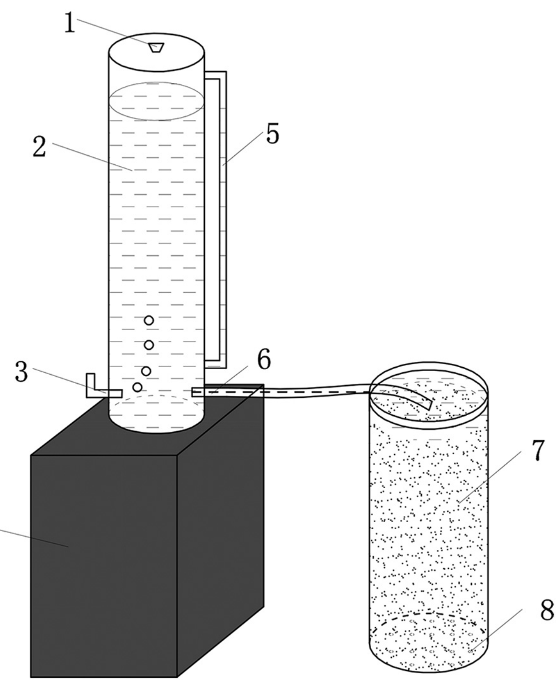

Fig. 3. The schematic diagram of the apparatus (note: 1 water inlet. 2 the Mariotte bottle. 3. air inlet. 4. the platform. 5. tape measure for water level reading. 6. water outlet. 7. simulated ring infiltrometer. 8. air entering passages.).

4. Results

4.1. Effects of the TSL on the measured infiltration rate

The infiltration rate curves f_e determined by a longer TSL were higher than those determined by a shorter TSL for the three experimental soil types especially in the initial infiltration stage (Fig. 4). For example, the initial infiltration rate of f_e at 10th min, measured at a TSL of 10 min, were 1.86–1.87, 1.87–2.29 and 3.19–4.39 times of those measured at a 1 min TSL for soils S1, S2 and S3, respectively (Fig. 5).

After the parameters in the Kostiakov model are estimated from the experimental data (Table 1), the Kostiakov model with specified regression parameters could well describe the infiltration rate values (AL-Kayssi and Mustafa, 2016). Fig. 6 showed the relationships between infiltration rates estimated by the Kostiakov model at 2 min and 5 min, 2 min and 10 min, respectively. The infiltration rates estimated at 10 min TSL were 1.30–1.61 times of those at 2 min TSL, indicating that the TSL significantly affected the measurement accuracy of entire infiltration process.

Among the three soil types, soil S3 was the most easily affected by TSL at which infiltration rate was measured (Figs. 5 and 6). This result can be attributed to the fact that soil S3 has the higher clay content. High clay contents promote crust and seal formation (Moldenhauer and Kemper, 1969; Valentin and Bresson, 1992; Mamedov et al., 2001), resulting in infiltration rate decreasing faster. The higher decreasing rate in infiltration rate indicated that the second part of the infiltration rate curves were more concave, resulting in its larger measurement error compared with soil S1 and soil S2.

In the analysis in Section 2.1, the actual infiltration rate at the 10 min TSL was even lower than that measured at a TSL of 1 min, but positioned at a later time moment made the infiltration rate higher. Therefore, the measurement system errors increased with increase in TSL. Decreasing the TSL may reduce the measurement error to a maximum degree.

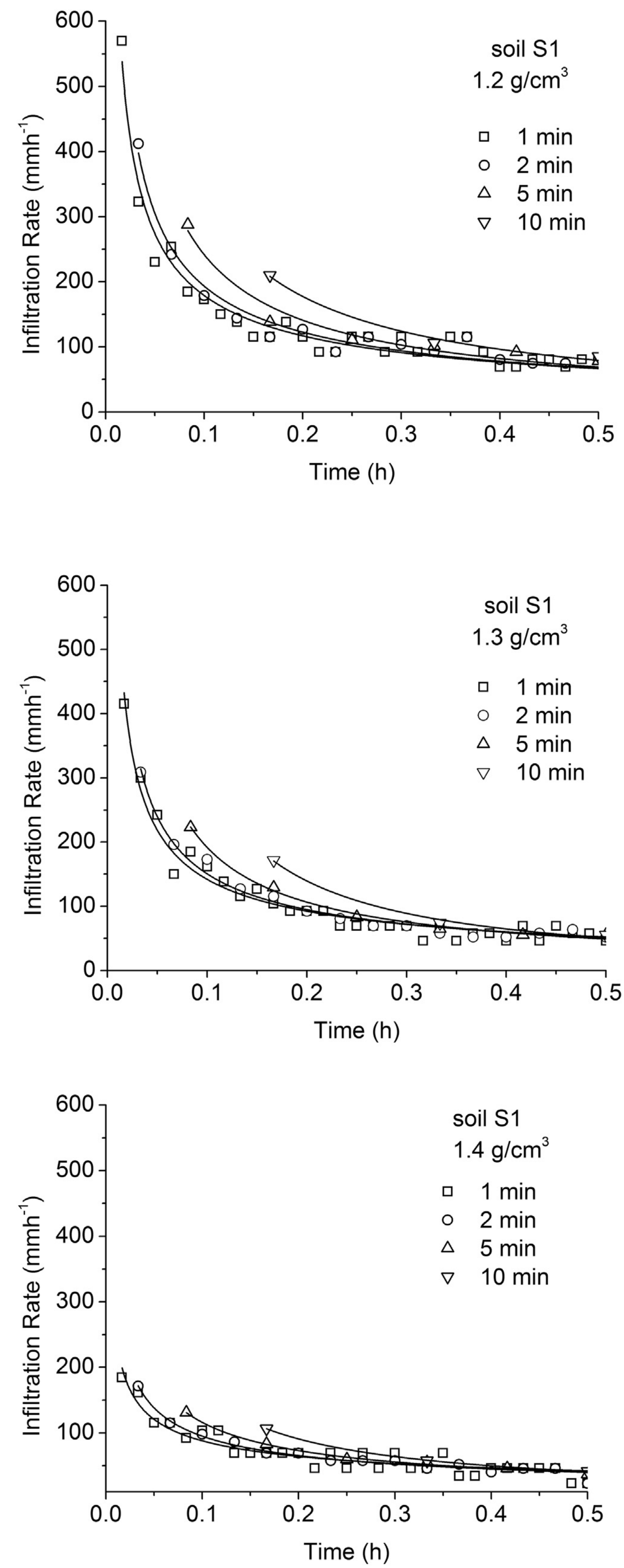

Fig. 4. Comparison of infiltration curves measured in different TSL as conventionally positioned at the end of the TSL.

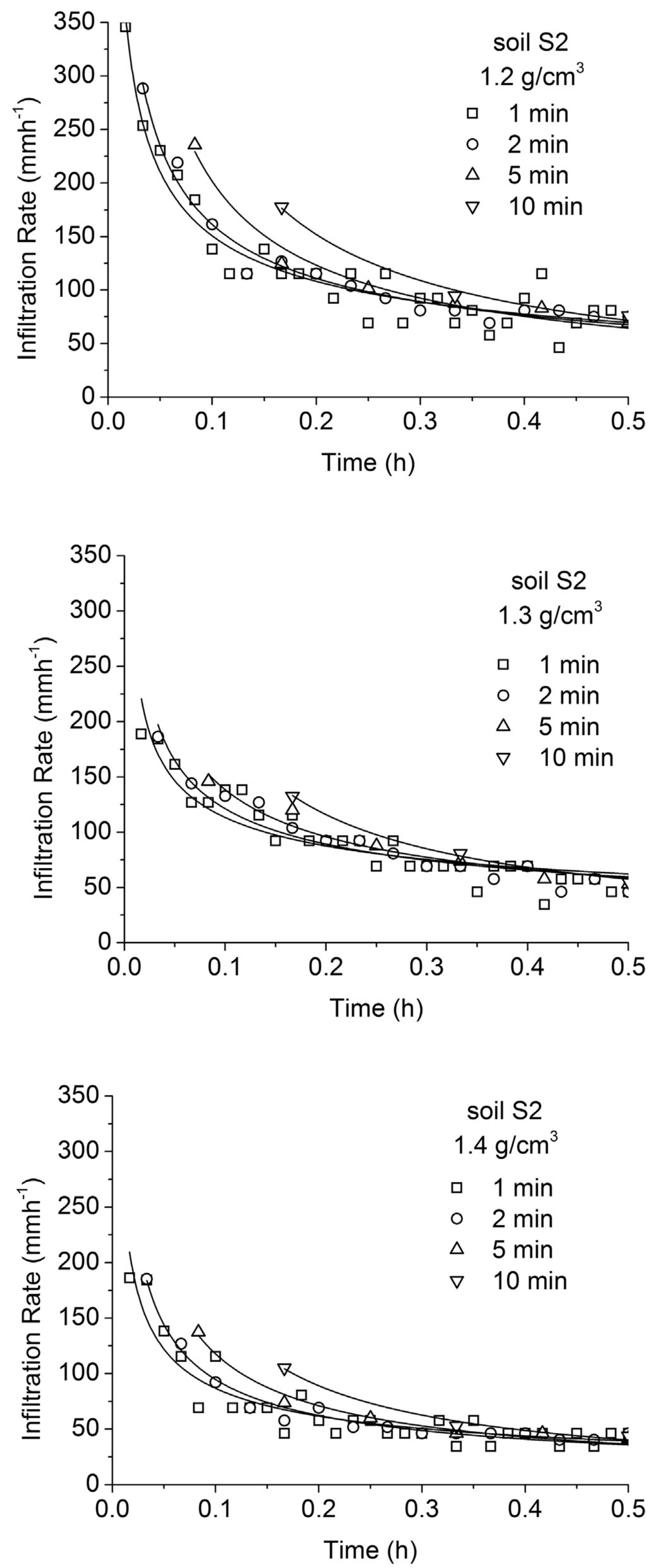

Fig. 4. (*continued*)

4.2. Errors in infiltration rate caused by reading the scale of the Mariotte bottle

Measuring the amount of infiltrated water at a specific period is necessary when measuring the infiltration rate (Franzluebbers, 2002; Verbist et al., 2013). The measurement error in infiltration rates caused

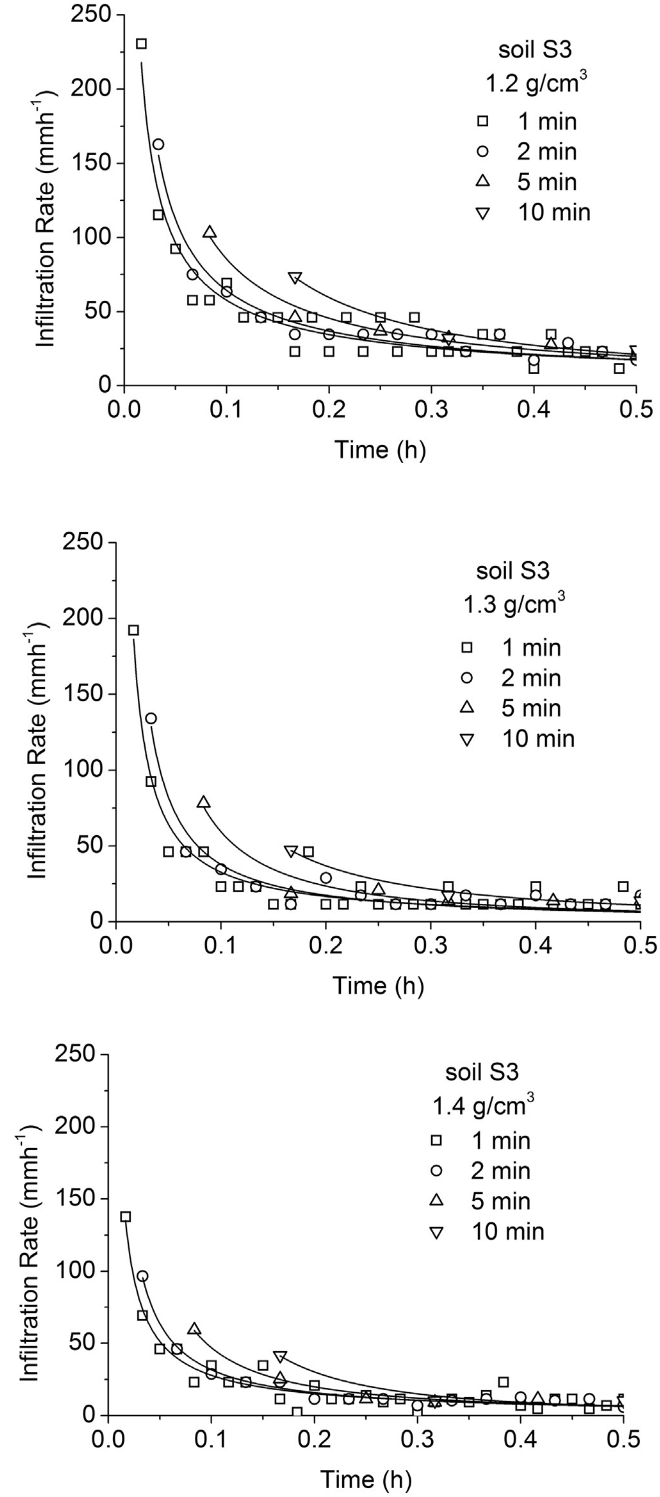

Fig. 4. (*continued*)

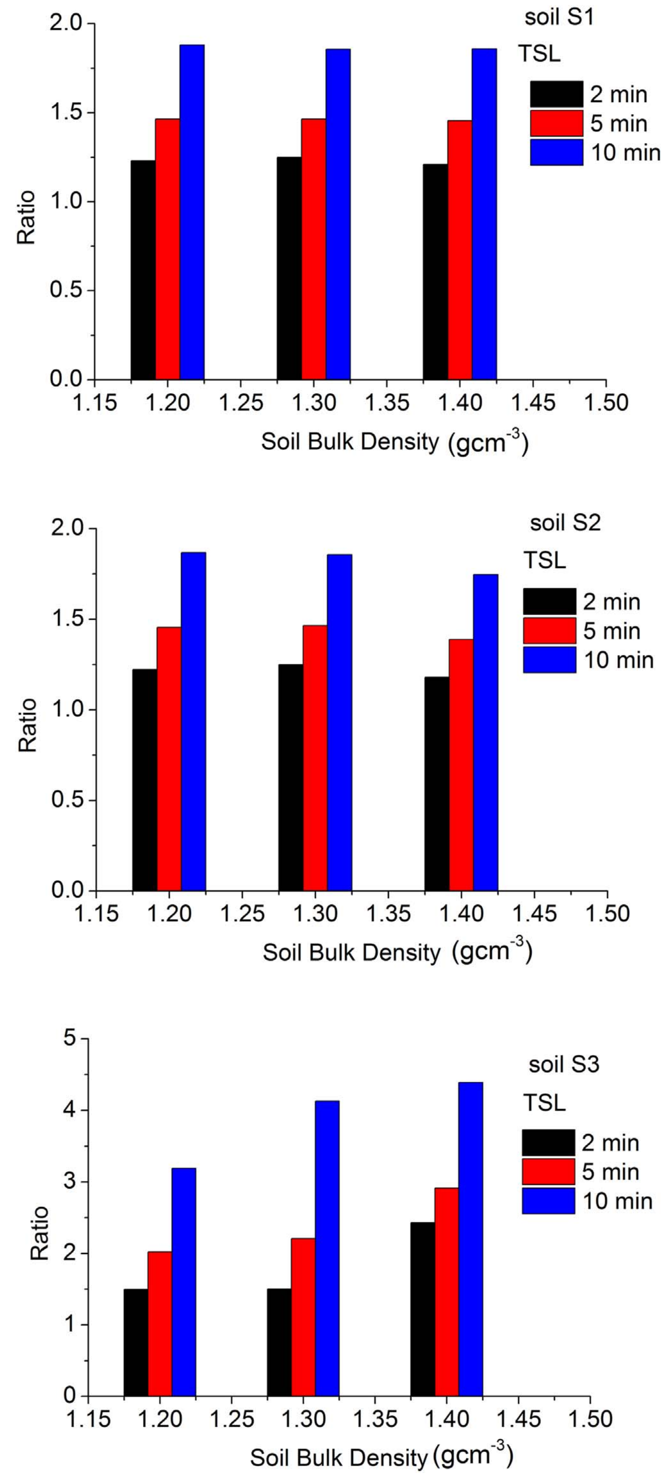

Fig. 5. Comparison of infiltration rates at the 10th minute measured at TSL of 2, 5, and 10 min with those at TSL of 1 min.

by the error in determining the water level is given by:

$$\delta_m = \left| \frac{\Delta H_m A_m}{i_t \Delta t A} \right| \times 100\% \tag{11}$$

where δ_m is the measurement error in infiltration rate caused by the reading error of water level, %; ΔH_m is the reading error of water level, L; A_m is the area of water supply cylinder, L^2; i_t is the transient infiltration rate at time t, L T^{-1}; Δt is the TSL, T; and A is the area of the infiltration ring, L^2.

In the various readings performed, the error in water level measurement generally ranged from -2 mm to $+2$ mm. With the assumption that the range of the initial infiltration rate was between 100 and 500 mm h^{-1}, the errors in infiltration rate measurement caused by the error in reading water level at different TSL (0.5, 1, 2, and 5 min) are shown in Fig. 7.

The error caused by the error in reading the water level increased with decreasing in TSL for the same infiltration rate from Fig. 7. Fig. 7(a) shows that the infiltration rate of 100 mm h^{-1} and a 0.5 min interval can result in an infiltration measurement error of 61.6%; this

Table 1
Model representation of soil infiltration rate curves.

Soil no.	Soil bulk density (g/cm^3)	PL	TSP (min)	Philip model			Kostiakov model		
				S	i_∞	R^2	a	b	R^2
S1	1.2	f_e	2	117.09	2.53	0.97	61.74	0.51	0.97
			5	136.64	− 2.20	0.94	64.21	0.53	0.95
			10	162.44	− 12.20	0.95	67.27	0.59	0.95
		f_m	2	86.00	21.43	0.972	62.32	0.42	0.98
			5	96.16	15.46	0.99	62.65	0.44	0.98
			10	99.07	14.59	0.99	69.07	0.43	0.99
		f_i	2	62.25	34.84	0.97	62.79	0.36	0.97
			5	37.51	47.54	0.95	65.33	0.28	0.99
			10	24.05	51.62	0.93	63.35	0.23	0.98
	1.3	f_e	2	93.98	− 5.62	0.93	38.90	0.59	0.95
			5	95.12	− 3.12	0.90	42.49	0.56	0.92
			10	103.20	− 4.12	0.88	46.15	0.57	0.89
		f_m	2	71.96	6.57	0.98	40.01	0.48	0.97
			5	73.75	6.31	0.95	41.82	0.48	0.94
			10	72.54	8.36	0.939	43.95	0.45	0.93
		f_i	2	46.98	22.25	0.98	42.76	0.39	0.99
			5	26.97	31.64	0.97	43.96	0.29	0.99
			10	16.07	37.49	0.97	44.65	0.22	0.99
	1.4	f_e	2	59.74	1.13	0.94	30.70	0.51	0.94
			5	72.49	− 4.60	0.96	30.89	0.56	0.97
			10	86.33	− 9.46	0.93	32.45	0.63	0.95
		f_m	2	49.67	6.22	0.95	30.81	0.45	0.95
			5	52.64	4.62	0.98	30.77	0.46	0.98
			10	56.27	3.42	0.98	31.24	0.47	0.98
		f_i	2	23.01	21.93	0.81	32.96	0.32	0.90
			5	25.72	14.81	0.84	32.52	0.26	0.93
			10	27.05	10.55	0.91	31.88	0.22	0.97
S2	1.2	f_e	2	103.36	− 0.38	0.97	50.89	0.51	0.97
			5	127.04	− 10.8	0.96	51.22	0.58	0.97
			10	150.69	− 20.45	0.96	53.15	0.63	0.98
		f_m	2	83.55	9.81	0.97	51.62	0.45	0.97
			5	84.52	9.53	0.991	51.64	0.45	0.99
			10	90.00	5.95	0.99	51.50	0.46	0.99
		f_i	2	50.46	28.50	0.89	53.38	0.35	0.95
			5	34.84	36.31	0.92	52.47	0.31	0.98
			10	23.31	40.70	0.97	51.94	0.25	0.97
	1.3	f_e	2	72.22	2.12	0.91	39.18	0.47	0.91
			5	94.80	− 9.02	0.98	38.29	0.57	0.98
			10	120.45	− 20.46	0.97	36.77	0.66	0.99
		f_m	2	60.09	8.93	0.90	39.35	0.42	0.92
			5	64.72	5.51	0.95	38.56	0.45	0.95
			10	70.74	1.76	0.99	37.35	0.48	0.99
		f_i	2	28.00	27.33	0.7	41.21	0.31	0.83
			5	16.45	32.95	0.67	40.31	0.25	0.82
			10	13.29	31.95	0.85	38.20	0.23	0.92
	1.4	f_e	2	64.67	− 5.46	0.96	26.43	0.56	0.96
			5	77.78	− 11.17	0.96	26.88	0.63	0.98
			10	92.97	− 17.18	0.96	27.50	0.70	0.98
		f_m	2	50.55	1.90	0.97	27.27	0.48	0.97
			5	52.84	0.71	0.99	27.25	0.49	0.99
			10	56.13	− 0.91	0.99	27.22	0.51	0.99
		f_i	2	17.05	22.00	0.77	29.88	0.31	0.90
			5	11.38	24.14	0.83	28.98	0.26	0.93
			10	7.81	24.65	0.88	27.44	0.22	0.94
S3	1.2	f_e	2	52.32	− 13.14	0.90	11.94	0.75	0.96
			5	56.81	− 12.87	0.91	13.95	0.78	0.96
			10	61.43	− 13.03	0.89	15.86	0.82	0.94
		f_m	2	42.33	− 7.74	0.96	13.22	0.63	0.98
			5	42.34	− 6.38	0.96	14.16	0.63	0.98
			10	42.49	− 6.11	0.97	14.56	0.63	0.98
		f_i	2	23.31	4.83	0.97	16.12	0.44	0.98
			5	13.99	8.30	0.94	15.98	0.35	0.96
			10	9.18	10.45	0.95	15.04	0.30	0.95
	1.3	f_e	2	32.62	− 9.14	0.79	5.50	0.86	0.90
			5	35.29	− 8.29	0.75	7.26	0.88	0.85
			10	37.26	− 7.65	0.83	9.71	0.82	0.89
		f_m	2	34.09	− 13.42	0.87	5.01	0.80	0.95
			5	31.74	− 9.50	0.86	5.43	0.80	0.95
			10	29.41	− 5.99	0.86	7.34	0.74	0.92
		f_i	2	17.93	− 0.63	0.97	7.99	0.52	0.97
			5	10.05	4.4	0.98	8.96	0.40	0.98
			10	5.65	6.65	0.97	9.42	0.30	0.97

(continued on next page)

Table 1 (continued)

Soil no.	Soil bulk density (g/cm^3)	PL	TSP (min)	Philip model			Kostiakov model		
				S	i_∞	R^2	a	b	R^2
	1.4	f_e	2	29.87	− 9.56	0.83	4.28	0.90	0.95
			5	30.03	− 7.39	0.79	5.96	0.89	0.89
			10	31.61	− 6.83	0.75	7.65	0.87	0.82
		f_m	2	24.63	− 6.85	0.90	5.15	0.74	0.96
			5	23.17	− 4.37	0.88	6.35	0.70	0.93
			10	23.77	− 4.40	0.86	6.56	0.73	0.90
		f_i	2	14.40	− 0.33	0.97	6.90	0.51	0.97
			5	8.40	3.57	0.97	7.52	0.40	0.97
			10	5.20	5.00	0.99	7.50	0.32	0.98

error was 10 times higher than that at a TSL of 5 min. Thus, the use of a short TSL yielded poor results in the initial infiltration stage.

Xie and Shen (1985) indicated that there existed an air-entry pressure at the water flow outlet of the Mariotte bottle, which also affects the infiltration measurement. The water only started to flow out of the bottle to supply water into the ring when the water level in the infiltration ring dropped to about 5 mm lower than the water flow outlet of the Mariotte bottle (Xie and Shen, 1985). This phenomenon could increase the relative error in the measured infiltration rate when the TSL for reading the water supply is shortened, to result in high fluctuations in the measured infiltration rate (Figs. 4 and 6). The maximum error of 5 mm within 0.5 min corresponded to an error of 600 mm h^{-1} in the computed infiltration rate. However, the error of 5 mm at a TSL of 5 min was reduced by 90%. Therefore, prolonging the TSL reduces the measurement error caused by reading the scale of the Mariotte bottle.

4.3. Comparison of infiltration curves positioned at the mid-point of TSL

The curves of f_m were almost identical, for the three soils in the test (Fig. 8). In the soil S1 of 1.2 g cm^{-3}, the infiltration rates measured at the fifth minute with TSL of 1, 2, and 10 min were 184.5, 161.4, and 177.8 mm h^{-1}, respectively, which were almost identical (Fig. 8).

The curves of f_m were comparable, but the infiltration rates measured at a short TSL fluctuated more than those measured at a long TSL for all the three soil types. This phenomenon may be attributed to the short TSL causing a higher relative error in reading compared with that in the long TSL, as discussed in Section 4.2. From a practical view, a long TSL (e.g., 5 min) and the middle PL of the TSL are recommended.

4.4. Estimation of measurement error

The relative error in the infiltration measurements can be estimated with the water balance and by comparing the actual supply of water with the estimated total infiltrated water. The relative error is given as:

$$\delta = \frac{Q_1 - Q_2}{Q_2} \times 100\% \tag{12}$$

where δ is the relative error, %; Q_1 is the computed infiltrated water, mm; and Q_2 is the total supplied water, mm.

The numerical integration over time was applied to compute the cumulative infiltration amount, Q_1 from the measured infiltration rate, which is theoretically determined as the total infiltration of water and is given by:

$$Q_1 = \int_0^T i(t)dt \tag{13}$$

where Q_1 is the computed infiltrated water, mm; and T is the total infiltration time, h.

The Philip model could not fit infiltration data using the f_i with lower R^2 (Table 1). Thus, in this study, $i(t)$ is a function of time as represented by the Kostiakov model. The actual infiltrated water Q_2 was measured by the changing water level in the Mariotte bottle.

The values of the initial error were all negative (− 31.74% to − 4.74%) (Table 2), indicating that the total infiltration amount calculated from f_i was lower than the actual infiltrated water and f_i underestimated the infiltration rate. However, f_e overestimated the infiltration rate, with the errors ranging from 7.48% to 155.87% (Table 2). The absolute value of the mid error is smaller than those of the end and initial errors among S1, S2, and S3 (Table 2). For soil S3 with a bulk density of 1.4 g cm^{-3}, the error of 10 min TSL reduced from 155.87% to 11.14% when the PL changed from the end point to midpoint of the TSL (Table 2). In addition, the absolute value of the error of midpoint PL has no relationship with the TSL, demonstrating that the midpoint PL could decrease the errors caused by the TSL. The infiltration rates measured by positioning the average infiltration rate at the midpoint of the TSL well approximated the true soil infiltration.

5. Discussion

The parameter S in the Philip model is called soil sorptivity, representing the soil's ability to absorb water (Philip, 1957b; Touma et al., 2007), which is an important soil property controlling water infiltration and movement into the unsaturated soil profile in the absence of gravity (Di Prima et al., 2016). In practical applications, S was estimated by fitting infiltration rate curves or cumulative infiltration curves over time with the Philip model (Liu et al., 2011; Kahlon et al., 2013; Ebel and Moody, 2016; Su et al., 2016).

To evaluate further the performance of f_m, Fig. 9 comparably showed S estimated by cumulative infiltration curves and f_i, f_m, and f_e. The S estimated by f_m was most consistent with that estimated by cumulative infiltration curves, with a proportional coefficient of 1.06 and a determination coefficient of 0.98. The parameter S estimated by f_e was larger than that of cumulative infiltration, with a proportional coefficient of 1.52; while f_i underestimates S, compared with that estimated by cumulative infiltration. f_m can more accurately estimate soil sorptivity.

The Kostiakov model can well describe infiltration curves because of the higher elastic parameters in the mathematical curve-fitting process (Silva, 2007). The parameter b represents the reduction speed in infiltration rate. Both a and b describe the infiltration rate at each moment. The fitting parameters of a and b in the Kostiakov model of f_m under different TSL were almost equal (Table 1), also indicating that f_m determined by different TSL was basically identical.

The Kostiakov model could also be used to express the cumulative infiltration process over time, as shown in Eq. (14),

$$I = At^B \tag{14}$$

where I is the cumulative infiltration (CI), L; A and B are the fitted parameters determined empirically; t is time, T.

Infiltration rate is the derivative of the cumulative infiltration to time, therefore a and A, b and B, in Eqs. (5) and (14) have the following relationships:

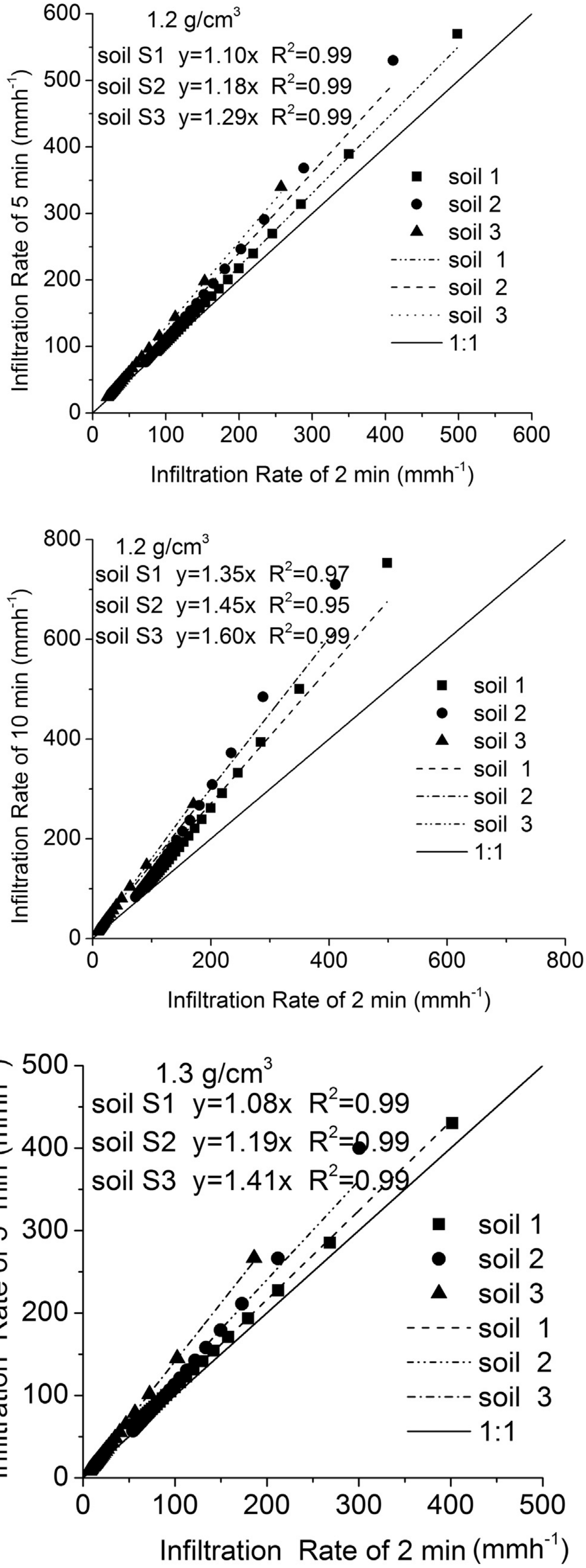

Fig. 6. Comparison of infiltration rates estimated by different TSL.

$$a = A \times B \tag{15}$$

$$b = 1 - B \tag{16}$$

The a and b estimated by the cumulative infiltration curves were

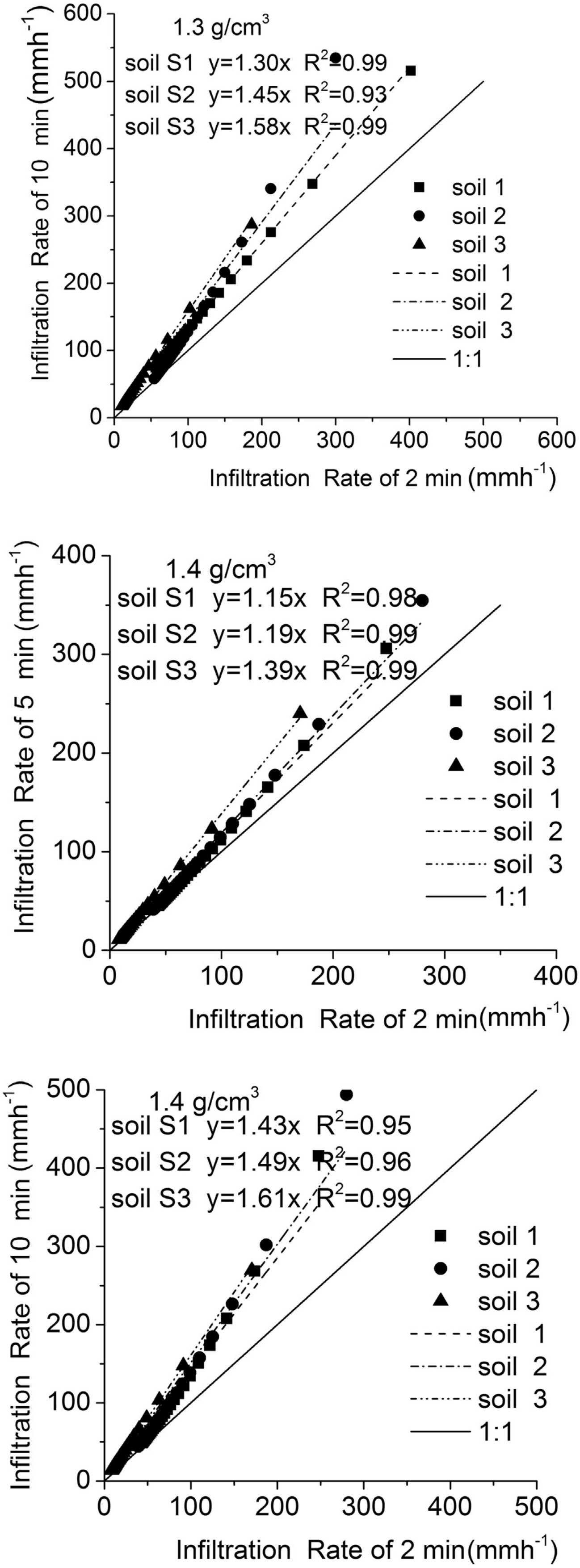

Fig. 6. (*continued*)

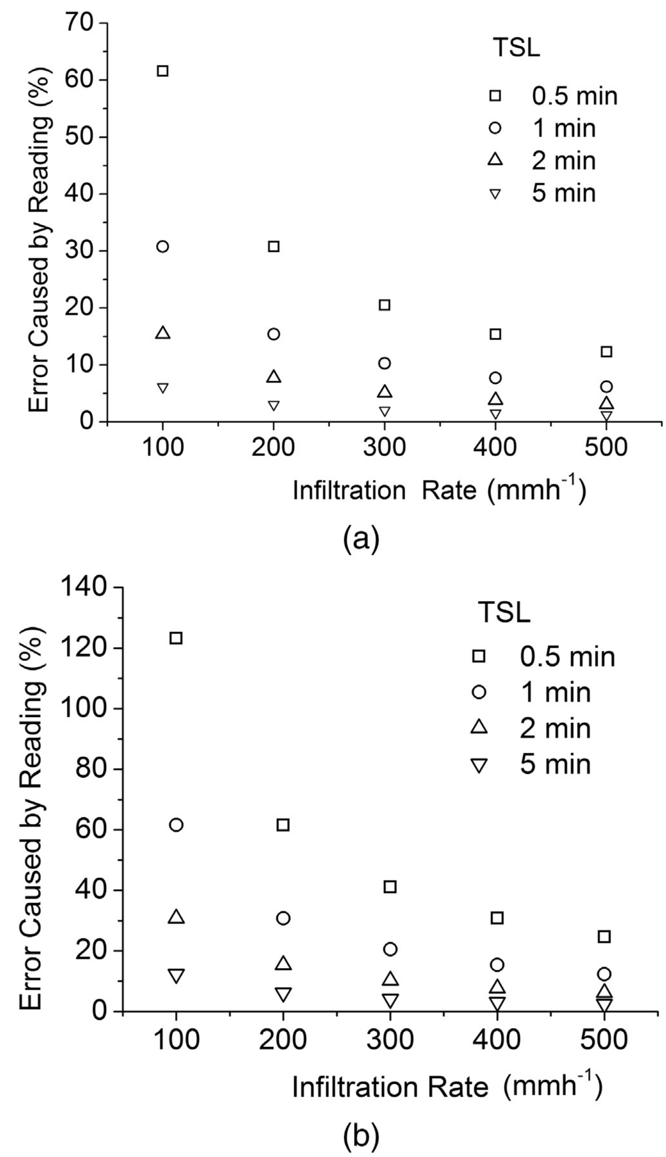

Fig. 7. Errors in the measured infiltration rate caused by reading errors in the Mariotte bottle in (a) ± 1 mm error of Mariotte bottle reading and (b) ± 2 mm error of Mariotte bottle reading.

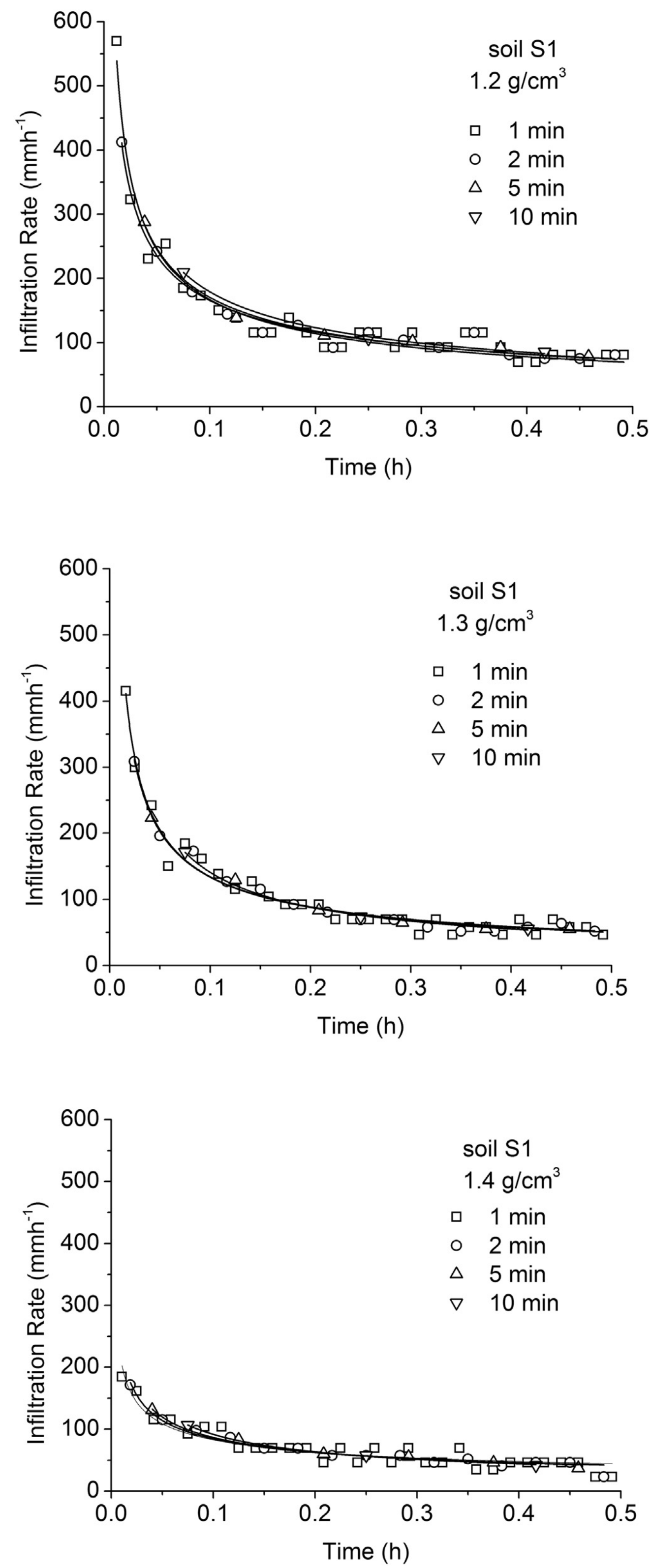

Fig. 8. Comparison of infiltration curves measured in different TSLs when positioned at the midpoint of the TSL.

compared with those estimated by f_m in Fig. 10. The results showed that the a and b value determined by f_m was very close to those estimated from CI, with proportional coefficients ranged from 0.97 to 1.11 and coefficient of determination greater than 0.8, indicating that f_m could well express the theoretical relationship between the infiltration rate and cumulative infiltration. Among the three TSLs, the proportional coefficient of 10 min was the one most close to 1, followed by that of 5 min and then that of 2 min.

These results also indicated that when a longer TSL was used, the parameters of f_m agreed well with those estimated with the cumulative infiltration curve. Under optimal conditions, the infiltration rate measured at an infinitely short TSL can infinitely approach the true infiltration rate. However, in actual measurement, decreasing the TSL could increase operational difficulties and cause large errors in reading the water level of the Mariotte bottle. As a result, infiltration measurement could produce large errors, causing that the proportional coefficient of a short TSL was a little far from 1, with a little lower coefficient of determination.

Nevertheless, the results indicated that the infiltration rate curves of f_m closely approximated each other. A long TSL can reduce error caused by reading the scale of the Mariotte bottle. Midpoint PL can reduce the system measurement error caused by the TSL. In this discussion, using an appropriate TSL, such as 5, or 10 min, and positioning the measured data at the midpoint of the TSL can simplify the operation and guarantee reasonable measurement accuracy.

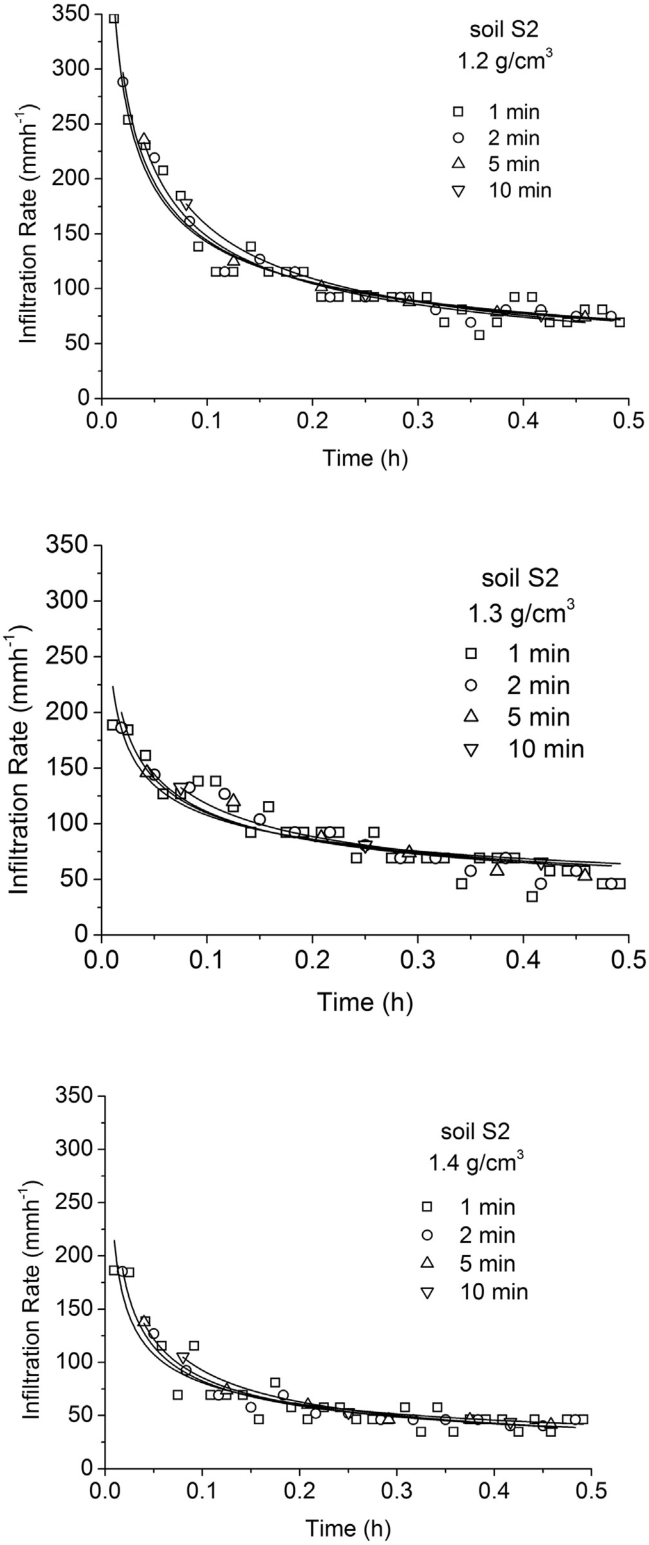

Fig. 8. (*continued*)

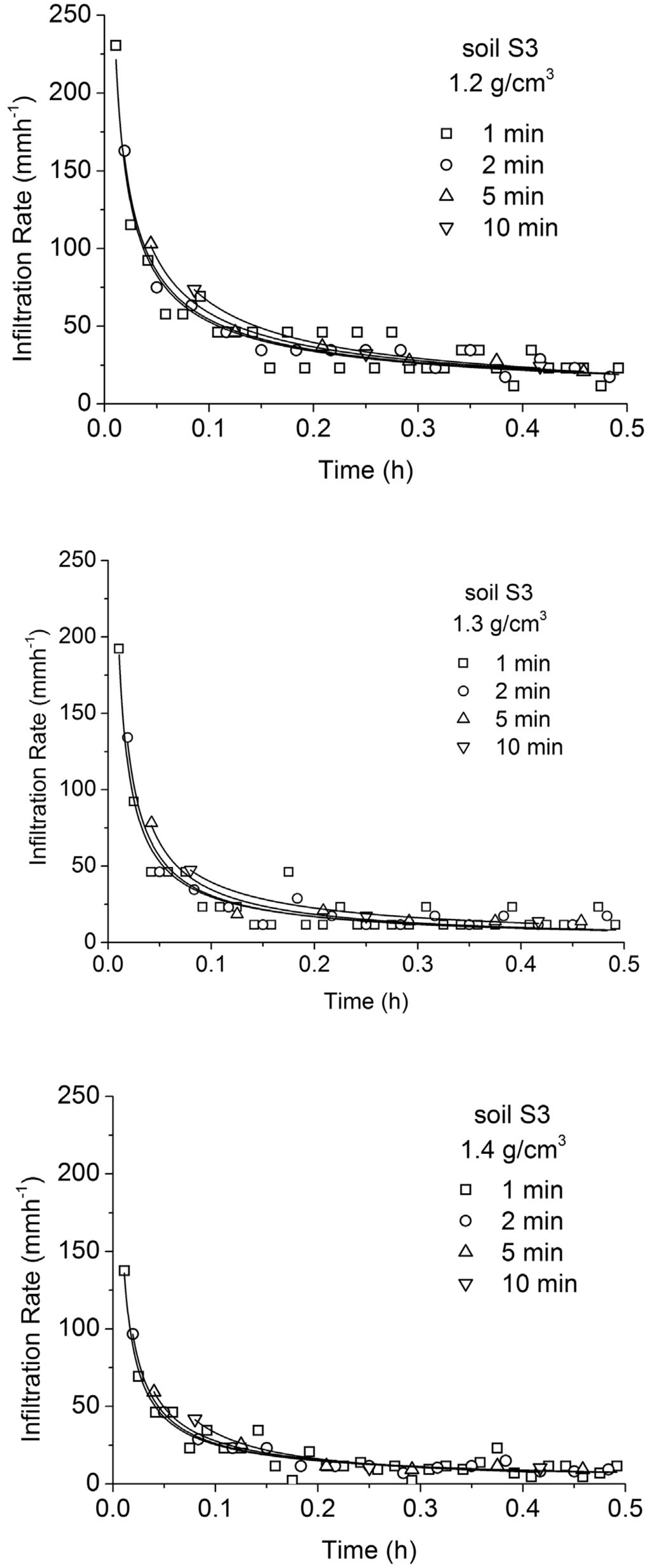

Fig. 8. (*continued*)

6. Conclusion

The effects of different TSLs and PLs on infiltration rates measured with a ring infiltrometer were quantitatively evaluated. Experiments were conducted in the laboratory by using three soils, four TSLs (1, 2, 5, and 10 min), and three PLs (initial, middle and end of a TSL). The infiltration rate using conventional PL (the end point of the TSL) increased with TSL increase. A short TSL can reduce the measurement error caused by the TSL. However, a short TSL leads to a higher measurement error caused by water level measurement error and increased operational difficulties. The relationships between infiltration rate curves measured by different TSLs were very close to each other when positioning the measured values at the mid-points of the TSLs, regardless of the TSLs (i.e. 1, 2, 5 or 10 min) used for the measurement,

Table 2
Errors in cumulative infiltration as calculated using the Kostiakov model with measured infiltration rates.

Soil no.	Soil bulk density (g/cm^3)	TSL (min)	End error (%)	Mid error (%)	Initial error (%)
S1	1.2	2	9.91	− 3.16	− 11.23
		5	17.53	2.00	− 13.95
		10	35.40	1.63	− 19.65
	1.3	2	8.96	− 4.64	− 10.38
		5	13.04	− 2.42	− 15.59
		10	24.16	1.23	− 21.75
	1.4	2	7.48	0.07	− 8.40
		5	16.33	1.19	− 17.07
		10	38.44	6.98	-21.04
S2	1.2	2	9.04	2.37	− 8.43
		5	21.97	2.64	− 14.72
		10	44.69	8.22	− 20.22
	1.3	2	9.32	3.88	− 4.74
		5	22.88	5.85	− 14.45
		10	56.54	5.49	− 20.10
	1.4	2	9.84	1.36	− 9.11
		5	26.55	4.76	− 15.00
		10	63.54	10.14	-25.00
S3	1.2	2	19.15	− 4.08	− 13.50
		5	54.93	0.34	− 21.73
		10	109.40	6.45	− 31.99
	1.3	2	43.36	1.11	− 24.44
		5	117.96	9.53	− 26.79
		10	101.97	8.55	− 29.65
	1.4	2	82.55	− 2.07	− 22.86
		5	132.58	6.78	− 26.31
		10	155.87	11.14	− 31.74

Note: end error represents the error calculated by f_e; mid error represents the error calculated by f_m; initial error represents the error calculated by f_i.

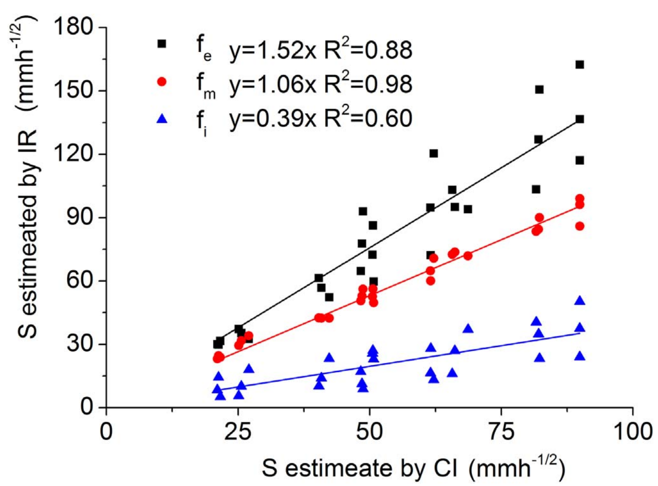

Fig. 9. Comparison between fitted values of S estimated by cumulative infiltration (CI) and infiltration rate curves (IR).

resulting in an error estimated by water balance lower than 12%, demonstrating that TSL is irrelevant when the measured infiltration rate is positioned at the midpoint of a TSL. Thus TSL should not be too short and a long TSL (5 min) is favorable as long as the measured data is positioned at the midpoint of a TSL. An appropriate TSL can reduce operational difficulties and errors in infiltration rate measurement caused by water level measurement error, and midpoint PL can considerably reduce measurement errors. The results of this study are valuable in the accurate measurement of soil infiltration.

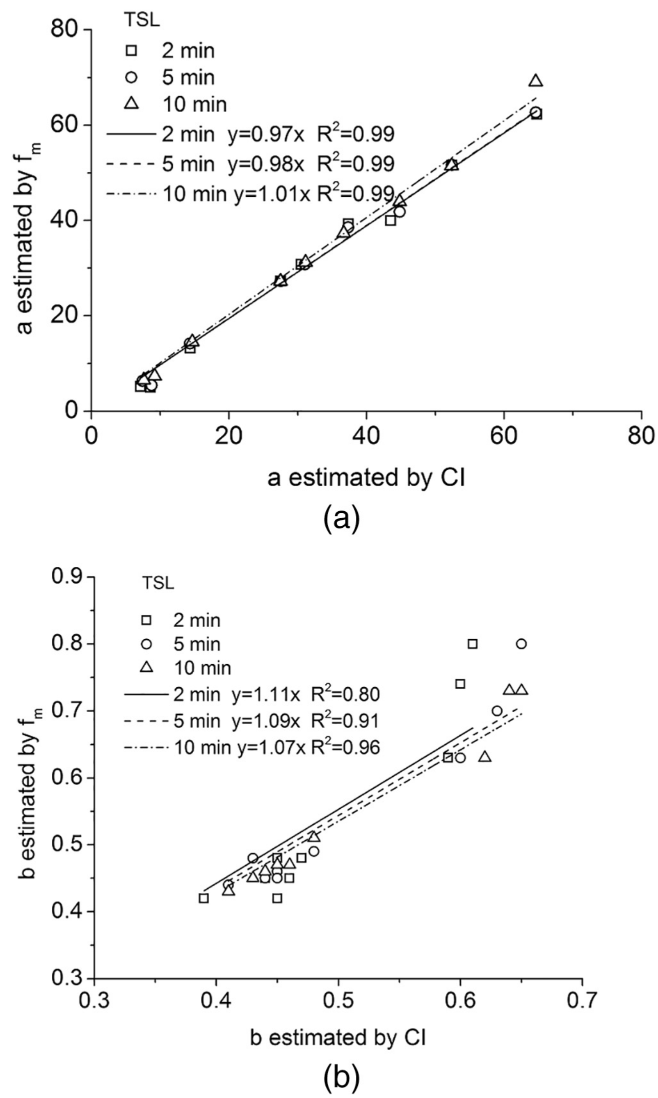

Fig. 10. Comparison of fitting parameters in the Kostiakov model estimated by f_m and CI.

Acknowledgements

This research was financially supported by the National Natural Science Foundation of China under project No. 41230746, and No. 51621061.

References

Adindu Ruth., U., Igbokwe Kelechi, K., Chigbu Timothy, O., Ike-Amadi, C.A., 2014. Application of Kostiakov's infiltration model on the soils of Umudike, Abia State-Nigeria. Am. J. Environ. Eng. 4 (1), 1–6.
AL-Kayssi, A.W., Mustafa, S.H., 2016. Modeling gypsifereous soil infiltration rate under different sprinkler application rates and successive irrigation events. Agric. Water Manag. 163, 66–74.
Anari, P.L., Darani, H.S., Nafarzadegan, A.R., 2011. Application of ANN and ANFIS models for estimating total infiltration rate in an arid rangeland ecosystem. Res. J. Environ. Sci. 5 (3), 236–247.
ASTM, 2003. D3385-03 Standard test method for infiltration rate of soils in field using double-ring infiltrometer. In: Annual Book of ASTM Standards 04.08. ASTM, West Conshohocken, Penn..
Bagarello, V., Sgroi, A., 2004. Using the single-ring infiltrometer method to detect temporal changes in surface soil field-saturated hydraulic conductivity. Soil Tillage Res. 76, 13–24.
Bagarello, V., Sferlazza, S., Sgroi, A., 2009. Comparing two methods of analysis of single-ring infiltrometer data for a sandy–loam soil. Geoderma 149 (3), 415–420.
Bamutaze, Y., Tenywa, M.M., Majaliwa, M.J.G., Vanacker, V., Bagoora, F., Magunda, M., Obando, J., Wasige, J.E., 2010. Infiltration characteristics of volcanic sloping soils on Mt. Elgon, Eastern Uganda. Catena 80, 122–130.
Berehe, F.T., Melesse, A.M., Fanta, A., Alamirew, T., 2013. Characterization of the effect of tillage on furrow irrigation hydraulics for the Dire Dawa Area, Ethiopia. Catena 110, 161–175.
Bodhinayake, W., Si, B.C., Noborio, K., 2004. Determination of hydraulic properties in sloping landscapes from tension and double-ring infiltrometers. Vadose Zone J. 3, 964–970.

Bouwer, H., 1986. Intake rate: cylinder infiltrometer. In: Klute, A. (Ed.), Methods of Soil Analysis. Part 1, second ed. Agron. Monog., vol. 9. ASA and SSSA, Madison, WI, pp. 825–844.
Carlier, E., 2007. A probabilistic investigation of infiltration in the vadose zone: proposal for a new formula of infiltration rate. Hydrol. Process. 21, 2845–2849.
Champatiray, A., 2014. Experimental Study for Determination of Infiltration Rate of Soils in Field Using Double Ring Infiltrometer. National Institute of Technology, Rourkela.
Chowdary, V.M., Rao, M.D., Jaiswal, C.S., 2006. Study of infiltration process under different experimental conditions. Agric. Water Manag. 83, 69–78.
Constantz, J., Murphy, F., 1987. An automated technique for flow measurements from Mariotte reservoirs. Soil Sci. Soc. Am. J. 51 (1), 252–254.
Di Prima, S., Lassabatère, L., Bagarello, V., Iovino, M., Angulo-Jaramillo, R., 2016. Testing a new automated single ring infiltrometer for Beerkan infiltration experiments. Geoderma 262, 20–34.
Ebel, B.A., Moody, J.A., 2016. Synthesis of soil-hydraulic properties and infiltration timescales in wildfire-affected soils. Hydrol. Process. 8, 1–17.
Eijkelkamp Company, 2012. Double ring infiltrometer operating instructions. Giesbeek, Nederland. https://www.eijkelkamp.com/files/media/Gebruiksaanwijzingen/EN/m1-0904eringinfiltrometer.pdf.
Franzluebbers, A.J., 2002. Water infiltration and soil structure related to organic matter and its stratification with depth. Soil Tillage Res. 66 (2), 197–205.
Green, W.H., Ampt, G.A., 1911. Studies on soil physics. J. Agric. Sci. 4, 1–24.
Hillel, D., 1998. Environmental Soil Physics. Academic Press, New York.
Horton, R.E., 1941. An approach toward a physical interpretation of infiltration-capacity. Soil Sci. Soc. Am. J. 5, 399–417.
Hou, R., Ouyang, Z., Li, Y., Tyler, D.D., Li, F., Wilson, G.V., 2012. Effects of tillage and residue management on soil organic carbon and total nitrogen in the North China Plain. Soil Sci. Soc. Am. J. 76, 230–240.
Iwanek, M., 2008. A method for measuring saturated hydraulic conductivity in anisotropic soils. Soil Sci. Soc. Am. J. 72 (6), 1527–1531.
Jury, W.A., Horton, R., 2004. Soil Physics. John Wiley & Sons, Inc., NJ.
Kahlon, M.S., Lal, R., Ann-Varughese, M., 2013. Twenty two years of tillage and mulching impacts on soil physical characteristics and carbon sequestration in Central Ohio. Soil Tillage Res. 126, 151–158.
Kostiakov, A.N., 1932. On the dynamics of the coefficient of water-percolation in soils and on the necessity for studying it from a dynamic point of view for purposes of amelioration. In: Transactions of 6th Committee International Society of Soil Science, Russia, Part A, pp. 17–21.
Kumar, B.V., 2014. Determination of Infiltration Rate of Soils Using Single and Double Ring Infiltrometer and Study of Drought Analysis in Karimnagar District of Andhra Pradesh. National Institute of Technology, Rourkela, pp. 20–23.
Lai, J., Ren, L., 2007. Assessing the size dependency of measured hydraulic conductivity using double-ring infiltrometers and numerical simulation. Soil Sci. Soc. Am. J. 71, 1667–1675.
Lei, T., Pan, Y., Liu, H., Zhan, W., Yuan, J., 2006a. A run off-on-ponding method and models for the transient infiltration capability process of sloped soil surface under rainfall and erosion impacts. J. Hydrol. 319, 216–226.
Lei, T., Liu, H., Pan, Y., Zhao, J., Zhao, S., Yang, Y., 2006b. Run off-on-out method and models for soil infiltration on hill-slope under rainfall conditions. Sci. China Ser. D Earth Sci. 49, 193–201.
León, J., Echeverría, M.T., Martí, C., Badía, D., 2015. Can ash control infiltration rate after burning? An example in burned calcareous and gypseous soils in the Ebro Basin (NE Spain). Catena 135, 377–382.
Liu, H., Lei, T., Zhao, J., Yuan, C., Fan, Y., Qu, L., 2011. Effects of rainfall intensity and antecedent soil water content on soil infiltrability under rainfall conditions using the run off-on-out method. J. Hydrol. 396 (1), 24–32.
Maheshwari, B.L., 1996. Development of an automated double-ring infiltrometer. Soil Res. 34 (5), 709–714.
Mamedov, A.I., Levy, G.J., Shainberg, I., Letey, J., 2001. Wetting rate, sodicity, and soil texture effects on infiltration rate and runoff. Soil Res. 39 (6), 1293–1305.
Mao, L., Lei, T., Li, X., Liu, H., Huang, X., Zhang, Y., 2008. A linear source method for soil infiltrability measurement and model representations. J. Hydrol. 353 (1), 49–58.
Moldenhauer, W.C., Kemper, W.D., 1969. Interdependence of water drop energy and clod size on infiltration and clod stability. Soil Sci. Soc. Am. J. 33 (2), 297–301.
Neris, J., Jiménez, C., Fuentes, J., Morillas, G., Tejedor, M., 2012. Vegetation and land-use effects on soil properties and water infiltration of Andisols in Tenerife (Canary Islands, Spain). Catena 98, 55–62.
Ogden, C.B., Van Es, H.M., Schindelbeck, R.R., 1997. Miniature rain simulator for field measurement of soil infiltration. Soil Sci. Soc. Am. J. 61, 1041–1043.
Oshunsanya, S.O., 2013. Spacing effects of vetiver grass (*Vetiveria nigritana* Stapf) hedgerows on soil accumulation and yields of maize–cassava intercropping system in Southwest Nigeria. Catena 104, 120–126.
Peng, X., Shi, D., Guo, H., Jiang, D., Wang, S., Li, Y., Ding, W., 2015. Effect of urbanisation on the water retention function in the Three Gorges Reservoir Area, China. Catena 133, 241–249.
Perroux, K.M., White, I., 1988. Designs for disc permeameters. Soil Sci. Soc. Am. J. 52, 1205–1215.
Peterson, A.E., Bubenzer, G.D., 1986. Intake rate: sprinkler infiltrometer. In: Methods of Soil Analysis. Part 1. Physical and Mineralogical Methods. American Society of Agronomy, Madison, WI, pp. 845–870.
Philip, J.R., 1954. An infiltration equation with physical significance. Soil Sci. 77, 153–158.
Philip, J.R., 1957a. The theory of infiltration: 1. The infiltration equation and its solution. Soil Sci. 83, 345–358.
Philip, J.R., 1957b. The theory of infiltration: 4. Sorptivity and algebraic infiltration equations. Soil Sci. 84, 257–264.
Philip, J.R., 1958. The theory of infiltration: 7. Soil Sci. 85, 333–337.
Philip, B.B., Wayne, C.H., 2002. Hydrology and Floodplain Analysis. Prentice-Hall, Inc., NJ, pp. 47–49.
Prieksat, M.A., Ankeny, M.D., Kaspar, T.C., 1992. Design for an automated, self-regulating, single-ring infiltrometer. Soil Sci. Soc. Am. J. 56 (5), 1409–1411.
Rasaily, R.G., Li, H., He, J., Wang, Q., Lu, C., 2014. Influence of no tillage controlled traffic system on soil physical properties in double cropping area of North China plain. Afr. J. Biotechnol. 11, 856–864.
Rashidi, M., Ahmadbeyki, A., Hajiaghaei, A., 2014. Prediction of soil infiltration rate based on some physical properties of soil. Am. Eurasian J. Agric. Environ. Sci. 14 (12), 1359–1367.
Ries, J.B., Hirt, U., 2008. Permanence of soil surface crusts on abandoned farmland in the Central Ebro Basin/Spain. Catena 72 (2), 282–296.
Ruggenthaler, R., Meißl, G., Geitner, C., Leitinger, G., Endstrasser, N., Schöberl, F., 2015. Investigating the impact of initial soil moisture conditions on total infiltration by using an adapted double-ring infiltrometer. Hydrol. Sci. J. 61 (7), 1263–1279.
Silva, L.L., 2007. Fitting infiltration equations to centre-pivot irrigation data in a Mediterranean soil. Agric. Water Manag. 94 (1), 83–92.
Su, L., Wang, Q., Shan, Y., Zhou, B., 2016. Estimating soil saturated hydraulic conductivity using the Kostiakov and Philip Infiltration equations. Soil Sci. Soc. Am. J. 11.
Touma, J., Voltz, M., Albergel, J., 2007. Determining soil saturated hydraulic conductivity and sorptivity from single ring infiltration tests. Eur. J. Soil Sci. 58 (1), 229–238.
Uloma, A.R., Samuel, A.C., Kingsley, I.K., 2014. Estimation of Kostiakov's infiltration model parameters of some sandy loam soils of Ikwuano-Umuahia, Nigeria. Open Trans. Geosci 1, 34–38.
Valentin, C., Bresson, L.M., 1992. Morphology, genesis and classification of surface crusts in loamy and sandy soils. Geoderma 55, 225–245.
Verbist, K., Cornelis, W.M., Torfs, S., Gabriels, D., 2013. Comparing methods to determine hydraulic conductivities on stony soils. Soil Sci. Soc. Am. J. 77 (1), 25–42.
Viessman Jr., W., Lewis, G.L., 1995. Introduction to Hydrology. Addison-Wesley Educational Publishers, Inc., Boston, pp. 52–53.
Woltemade, C.J., 2010. Impact of residential soil disturbance on infiltration rate and stormwater runoff. J. Am. Water Resour. Assoc. 46, 700–711.
Xie, S.Z., Shen, Y.L., 1985. Improvement and application of Mariotte bottle. Hydrogeol. Eng. Geol. 2, 18–19 (in Chinese).